

Chessboard-Like High-Frequency Patterns for 3D Measurement of Reflective Surface

Zaixing He^{ID}, Senior Member, IEEE, Peilong Li^{ID}, Xinyue Zhao^{ID}, Lianpeng Kang^{ID},
Shuyou Zhang^{ID} and Jianrong Tan^{ID}

Abstract—Surface reflections severely degrade the performance of the structured-light 3D measurement. In this article, we introduce a novel structured-light 3D measurement technique that works in the presence of reflective highlights. The focus of this article is on designing chessboard-like coding schema and crossover-based decoding schemes. First, we design chessboard-like fringe patterns that are resistant to reflective highlights by using simple logical operations. Compared with conventional coding schemes that inevitably have low-frequency patterns, the chessboard-like coding schemes use all-high-frequency patterns to provide a better highlights-suppression effect. Second, we propose an inverse-pattern method to extract crossover positions for decoding. The chessboard-like patterns have abundant crossover information. The crossover information is more localizable and better preserved than image intensity, which makes the decoding strategy more robust. Moreover, both positive and negative patterns are used to precisely localize the crossover positions. The proposed method can be readily incorporated into existing binary structured-light measurement techniques without significant overhead in terms of capture time or hardware. Extensive experiments are shown to demonstrate the high performance of the proposed method.

Index Terms—Global illumination structured-light 3D measurement, surface reflections.

I. INTRODUCTION

WITH the development of industrial automation, graphics, and human-computer interaction, there is an increasing demand for structured-light 3D measurement in the industry. In this field, a sequence of fringe patterns is projected onto the target object and the resulting fringe patterns on the object surface are captured by a camera. Due to the height of the object, the captured images are deformed. According to the principle of triangulation, by analyzing how the fringe patterns are deformed, the 3D shape (depth information) can be computed. In the last decade, significant processes made by related research are mainly focused on two aspects: the

Manuscript received March 21, 2021; accepted April 16, 2021. Date of publication April 22, 2021; date of current version May 12, 2021. This work was supported in part by the National Natural Science Foundation of China under Grant 51775497 and Grant 51775498 and in part by the Zhejiang Provincial Natural Science Foundation under Grant LY21E050021. The Associate Editor coordinating the review process was Dr. Emanuele Zappa. (Corresponding author: Xinyue Zhao.)

The authors are with the School of Mechanical Engineering, the State Key Laboratory of Fluid Power and Mechatronic Systems, Zhejiang University, Hangzhou 310027, China (email: zaixinghe@zju.edu.cn; lplzju18@zju.edu.cn; zhaoxinyue@zju.edu.cn; Lianpeng_kang@zju.edu.cn; zsy@zju.edu.cn; egi@zju.edu.cn).

Digital Object Identifier 10.1109/TIM.2021.3075035

reduction of measurement time [1], [2] and the enhancement of measurement accuracy [3], [4], [21].

Despite these advances, these techniques assume that the deformed fringe pattern is available for all parts of the object. This is true only when all parts of the object surface have homogenous reflectivity of light. However, for many real-world scenarios, objects are made of materials with nonhomogenous reflectivity of light, such as metal, porcelain, etc. For example reflections are ordinary and universal in the industry. Especially in highprecision manufacturing, objects are generally reflective, as they usually have low surface roughness. On the reflective object surface, some areas receive overwhelming illumination from various directions and become shiny or reflective. This corrupts the fringe pattern and compromises the quality of the captured image; thus, it compromises the 3D measurement results.

Hence, in the presence of highlights, existing intensity-based structured-light methods virtually encounter difficulties, which is a challenging task and has been an active research focus recently. To address this task, existing solutions can be divided into four aspects.

One solution is to suppress the reflective nature of the shiny surface in an exclusive hardware means. The common practice is to coat the shiny surface with a thin layer of opaque powder to suppress the reflective nature of the shiny surface. However, such an additional coating film may cause corruptions to the target surface, which leads to a distinct effect on the final measurement accuracy [5]. Another method is to capture several fringe images from multiple viewpoints by using a moving camera or a moving scene [8], [14], [19]. Highlights could be somewhat reduced with these techniques. Nevertheless, it comes at the cost of additional hardware requirements and complicated calibration procedures.

The second solution is to inpaint (restore) the fringe images distorted by the reflective highlights in postprocessing. The method in [6] requires the illumination information, including the observed pixel colors, highlight color analysis, and illumination color uniformity, for guiding the inpainting procedure. The method in [7] requires the geometrical structure of the fringe patterns for guiding the iterative inpainting procedure. The essence of inpainting is an imprecise guess with experience. It works well when the object surface complies with experience. However, this experience-based technique encounters difficulties when the object surface disagrees with the experience (for example, an unexpected patterned

surface). Therefore, it cannot be straightforwardly applied to the high-accuracy measurement. Moreover, because of the complex nature of the reflective highlights, the inpainting process is computationally expensive and takes prohibitive time [15], [16].

The third solution is to use multiple fringe images of different fringe patterns. For instance, the method in [9] attempts to employ the high-frequency fringe patterns to separate and remove the highlights (global components). However, this separation method may lead to undesired artificialities (additional residues) in the measured fringe patterns, and have a significant increase in the number of fringe patterns. Instead of separating the highlights, the methods in [10], [11], [17], and [18] take advantage of the nature of the high-frequency illumination for highlights suppression. These methods redesign coding schemes so that only high-frequency fringe patterns are required for measurement. While this technique has shown promise, it suffers from the drawback that they need a significantly higher number of fringe patterns than conventional methods, or the residual results after highlights suppression are too noisy.

The fourth solution is the phase measuring deflectometry. In this solution, a screen is used to display sinusoidal fringe patterns and a camera is used to observe the fringe images reflected from the measured specular surface [12], [13], [20]. However, to obtain clear reflected images this solution requires the measured objects' surface to have pure specular reflections. Therefore, this solution is only suitable for the object with an extremely smooth surface such as the mirror and the optical lens. Whereas, most reflections are between the specular reflections and diffuse reflections.

In this article, we introduce a novel structured-light 3D measurement technique that works in the presence of reflective highlights. The focus of this article is on designing a chessboard-like coding schema and crossover-based decoding schemes. In particular, we consider binary structured-light patterns, which are perhaps the simplest to implement and widely used in a plethora of research and commercial systems.

As for the coding schemes, the key observation is that high-frequency illuminations can alleviate the reflective highlights [10]. On the other hand, low-frequency illuminations result in significant highlights, making it hard to decode them reliably. Hence, we design and project fringe patterns with only high frequency. The key idea is to express low-frequency patterns as pixel-wise logical combinations of a high-frequency pattern. In comparison, most currently used patterns (e.g., gray-code patterns) contain both low and high spatial frequencies, and thus are ill-equipped to deal with the reflective highlights.

As for the decoding schemes, as the well-designed chessboard-like patterns in coding schema implies plentiful localizable and reliable crossover position, we use the crossover position but not the individual image intensity to extract coded information. The crossover position is obtained by the use of both positive and negative patterns and a zero-crossing crossover detector. In this way, the crossover is more precise and distinguishable as compared to the raw image intensities, albeit in the presence of influence from the specular

nature of the target scene to the overall captured image's intensity distribution. Moreover, as the positive and negative patterns have the same frequency, they produce constant global illumination for each point in the scene. This enables the high robustness of the decoding schemes.

Above all, the proposed method is aiming at making 3D measurement techniques practical for real-world reflective scenarios. The contribution of the proposed method is threefold

- 1) For the coding schema, we design chessboard-like fringe patterns that diminish reflective highlights and prevent the errors at capture time itself. Different from existing gray-code-like patterns that have high-frequency changes in a single direction, the chessboard-like patterns are more resilient to highlights as it has multi-directional high-frequency changes. To the best of our knowledge, it is the first time to employ chessboard-like fringe patterns for structured-light measurement.
- 2) For the decoding schema, we propose an inverse-chessboard-like-pattern method to extract crossover positions for decoding. The use of both positive and negative (inverse) chessboard-like patterns provides plentiful localizable crossover, which enhances robustness and localizability in decoding, as these two patterns remain constant (same) highlight (reflective) components that can be removed by a difference operation. Moreover, we use crossover information for extracting coded information. This makes decoding robust as the crossover information is more localizable and better preserved than image intensity in the presence of reflections.
- 3) We prevent the adverse effect of reflective highlights in both coding and decoding procedures. In contrast, conventional methods mainly focus on improvements in the coding procedure. This makes the proposed method outperforms the state-of-the-art highlights-suppression methods.
- 4) The remainder of this article is organized as follows. Section II describes the proposed patterns for highlights prevention. The decoding algorithm by using inverse patterns and a crossover detector is presented in Section III. Experimental results are given in Section IV. Conclusions are presented in Section V.

II. CHESSBOARD-LIKE CODING SCHEMA FOR REFLECTIVE HIGHLIGHTS PREVENTION

In this section, we describe the details of pattern designs (coding schemes), and analyze the suppression effect of high-frequency illumination on reflective highlights.

A. Proposed Coding Schemes

To minimize the reflective highlights and prevent errors at capture time itself, we aim to design coding patterns with only high frequencies. However, conventional commonly used patterns contain a combination of both low and high frequencies. The method in [10] proposed a design of high-frequency-only patterns, but it complicates the decoding algorithms. In the proposed coding schemes, we employ logical operations to make it possible to generate patterns with only

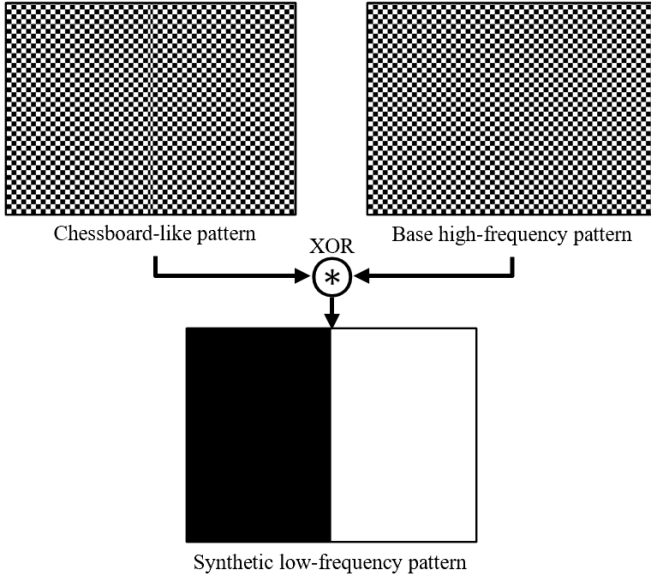


Fig. 1. Proposed coding schema. Different from conventional gray-code coding schema, the proposed schema enables an arbitrary gray-code patterns (see the low-frequency pattern in the second line) to be divided into two high-frequency patterns. Based on the proposed schema, any sequences of conventional gray-code patterns can be equally converted to a sequence of chessboard-like patterns plus a base high-frequency pattern. In other words, there is no need to project low-frequency patterns which would be further experimentally demonstrated to be vulnerable to reflective highlights. The proposed schema. In real practice, we use the edge position instead of the binarized intensity for decoding. In the proposed logical coding schemes, a low-frequency pattern is expressed as a pixel-wise logical combination (e.g., XOR) of two high-frequency patterns. Only high-frequency patterns are projected on the object surface. Then the two captured images are combined by performing another pixel-wise XOR operation, which produces the correct binarization as if the surface was projected by the conventional low-frequency pattern but removes the reflective highlights.

high frequencies, and make sure the decoding algorithm is as simple (cost-efficient) as convention Gray-code methods. To make sure the frequency as high as possible, rather than the stripe patterns in general, the proposed patterns are designed to look like a chessboard.

Fig. 1 shows an example of the proposed patterns. The binary structured-light patterns are considered in our implementation. For binary structured-light techniques, we binarize the captured images to enable the further decoding procedure. For the convenience of expression, we represent the binary fringe patterns as P , and define the binarization process of the captured image which is illuminated by P as $b(*)$. Hence, the binarized segmentation results of the underlying captured images which is illuminated by P can be expressed as $b(P)$.

As discussed in Section I, in presence of reflective highlights, $b(P)$ can be robustly obtained if P is a high-frequency pattern. On the other hand, if P is a low-frequency pattern, $b(P)$ may be incorrectly computed. To make sure all patterns have high frequencies, we decompose an arbitrary low-frequency pattern P_l into two high-frequencies P_{h1} and P_{h2} via a pixel-wise binary logic operation

$$b(P_l) = b(P_{h1} P_{h2}) = b(P_{h1}) b(P_{h2}). \quad (1)$$

If such an operation can be found, we can use the two binarizations $b(P_{h1})$ and $b(P_{h2})$ to compute a correct binarization

$b(P_l)$. Fortunately, we find that the logical XOR operation satisfies the requirement in (1). This is easy to prove, as $P P = 0P = P$ and $(PQ) R = P(Q \otimes R)$, for arbitrary patterns P , Q and R . This property makes it possible to decompose a low-frequency pattern into two high-frequency patterns, and ensure that no low-frequency patterns are required to be projected anymore. In the meantime, as we can compute and combine two high-frequency binarizations to achieve an equivalent low-frequency conventional patterns, which makes the further decoding schemes are as convenient and straightforward as conventional methods, which does not complicate the further decoding schemes.

According to (1), all high-frequency patterns can be transferred from not-all-high-frequency patterns in the following procedures. First, we choose a high-frequency patterns P_{h1} as a base pattern. In particular, the base pattern is selected as a chessboard pattern that has high-frequency in multiple directions and provides excellent antihighlights performance. Second, for each pattern P_l in the not-all-high-frequency patterns, by taking the pixel-wise logical XOR of P_l and P_{h1} , we can obtain a set of high-frequency patterns P_{h2} . After this, instead of the low-frequency pattern P_l , we project the two high-frequency patterns P_{h1} and P_{h2} . And the original low-frequency pattern P_l still can be achieved by performing another pixel-wise logical XOR operation. In this way, as the binarizations $f(P_{h1})$ and $f(P_{h2})$ are correct, the XOR result $f(P_l) = f(P_{h1}) f(P_{h2})$ is also correct, which mediates the contradiction between the low-frequency pattern and reflective highlights, as shown in Fig. 1. In our practice, we take the typical not-all-high-frequency pattern, the conventional gray-code patterns, as an example, because it is widely used in a plethora of research and commercial systems.

Fig. 2 shows the comparison of conventional gray-code patterns and the proposed high-frequency patterns. The proposed patterns can be constructed by taking the pixel-wise logical XOR of a high-frequency pattern (base pattern) with conventional gray-code patterns. In particular, the base pattern is a high-frequency stripe pattern whose intensity-change direction is orthogonal to that of the Gray-code patterns. The proposed patterns have only high frequencies. The number of projected patterns only increases by 1. The base pattern provides access from the proposed high-frequency patterns to conventional not-all-high-frequency patterns like the gray-code patterns. This makes the decoding schemes remain the same simple and convenient, which does not require complicated decoding algorithms.

B. Analysis of High-Frequency Illumination

The basic principle behind the proposed coding schemes is the highlights-suppression effect of high-frequency illumination. As shown in Fig. 2, the highlights under the high-frequency illuminations are much less than that under the low-frequency illuminations, which lead to a more accurate and robust decoding result.

The reflective highlights result in incorrect binarization results (incorrect decoding results), and then add adverse effects on the depth measurement results. These reflective

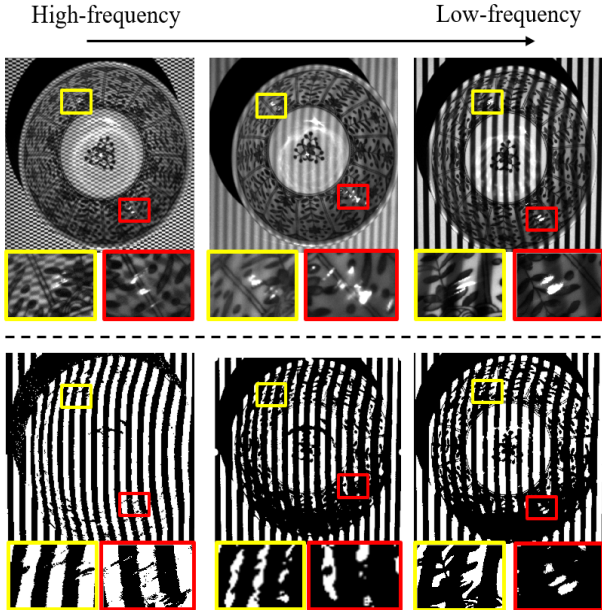


Fig. 2. Changes of highlights and decoding results under the frequency variances. High-frequency projection provides highlights-suppression images and better binarization results. Captured images under different illumination frequencies (top). Underlying decoding results under different illumination frequencies (bottom). As the frequency decreases, the reflective highlights become more and more distinct, which results in more inaccurate decoding results, and vice versa. Compared with low-frequency illuminations, high-frequency illuminations have a better highlights-suppression effect and lead to the most accurate decoding result.

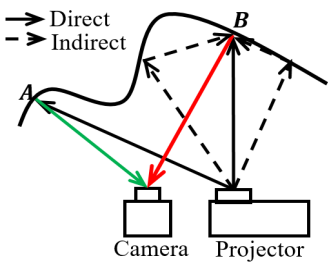


Fig. 3. Causes of interreflections. The scene point B receives overwhelming indirect illuminations from other scene points over a large region and form highlights in the captured image (see the red line). On the other hand, there are no highlights in the captured image (see the green line) if a scene point (see A) receives only direct illumination. Hence, the way to prevent highlights is to remove the indirect illumination component.

highlights arise from interreflections. That is, a scene point may receive overwhelming indirect illuminations from other scene points over a large region and form highlights, as shown in Fig. 3. Compared with low-frequency illuminations, high-frequency illuminations are less subject to highlights [see Fig. 2 (top)], and the underlying decoding results contain more missing areas [see Fig. 2 (bottom)]. To prove this, we analyze the effect of highlights on binary structured light.

Binary patterns are coded by binarized 1 (ON) and 0 (OFF) pixels, and decoded by binarizing the captured images into *lit* versus *nonlit* pixels. A robust way to do this is to capture two images L and \bar{L} , under the positive pattern P and the negative pattern \bar{P} , respectively (see Fig. 4). For a scene point S^i we compare its irradiances L^i and \bar{L}^i . If $L^i > \bar{L}^i$, then the

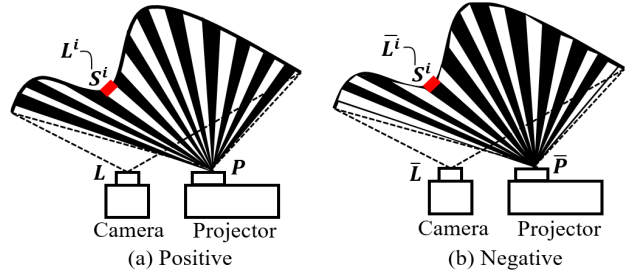


Fig. 4. Positive illuminations and negative illuminations. The source radiates high-frequency binary patterns, including (a) positive pattern P and (b) underlying negative pattern \bar{P} , resulting in two captured images L and \bar{L} respectively. The lit patches in (a) include both direct and indirect components, while the unlit patches in (b) include only an indirect component.

point is classified as directly lit. The assumption for correcting binarization is that each scene point receives irradiance from only a single illumination element (projector pixel). However, due to interreflections, a scene point receives irradiance from multiple projector pixels, leading to incorrect binarization.

In the presence of interreflections (reflective highlights), suppose S^i is directly lit under a pattern P the irradiances L^i and \bar{L}^i are

$$\begin{cases} L^i = L_d^i + \beta L_g^i \\ \bar{L}^i = (1 - \beta)L_g^i \end{cases} \quad (2)$$

where L_d^i and \bar{L}_d^i are the direct components and indirect components of the irradiance at S^i , when the scene is fully lit. β is the fraction of the indirect component under the pattern P .

Based on the correct binarization condition, $L^i > \bar{L}^i$ for correct binarization, we have

$$L_d^i + \beta L_g^i > (1 - \beta)L_g^i. \quad (3)$$

This condition is satisfied with the high-frequency illumination. Hence, the captured image is binarized correctly even in the presence of highlights due to interreflections. We will explain this as follows.

If the scene is illuminated with an ideal high-frequency pattern (with equal ON and OFF pixels), we have $\beta \approx 0.5$, as discussed in [9]. Thus, for a scene point S^i , $L^i \approx L_d^i + 0.5L_g^i$ and $\bar{L}^i \approx 0.5L_g^i$. Consequently, we have $L^i > \bar{L}^i$ and the condition for correct binarization is satisfied.

On the other hand, we consider $\beta \approx 0$ (a scene point S^i receives most of the indirect component when it is not directly lit), and $L_d^i < L_g^i$ (the indirect component is larger than the direct component). Such a situation is true when a scene is illuminated with a low-frequency pattern (asymmetrically illumination) and in the presence of reflective highlights [9]. Substituting in (3), we have $L^i < \bar{L}^i$ which is not satisfied with the correct binarization condition. Hence, binarization error occurs in the reflective (highlight) scene points.

In comparison to the traditional gray-code-like coding schemes, the proposed chessboard-like coding schemes have a higher frequency and hence have a better highlights-suppression effect. An example is shown in Fig. 2.

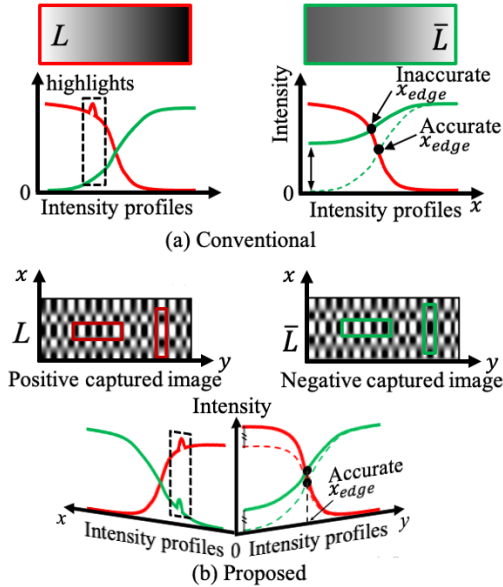


Fig. 5. (a) For conventional coding schema, with surface reflection, captured images (intensity profiles) in positive and negative captured images are asymmetrically distorted by the highlights, leading to inaccurate edge detections. (b) Proposed method changes its patterns in high-frequency along both x and y directions, which enables high-frequency illuminations in two dimensions. On the contrary, the conventional method has pattern changes in only one direction, and these changes are low frequency. As (4) only holds true under high-frequency illuminations, the proposed method can eliminate indirect illumination component (reflective highlights) by subtracting the positive and negative images. Hence, the proposed inverse-pattern method and stripe detection method can resist the interference of reflective highlights, as the high-frequency nature ensures that the reflections have a symmetrical influence on positive and negative chessboard-like patterns, which enable the elimination of reflections by subtracting the two inverse captured images.

III. INVERSE-CHESSBOARD-LIKE-PATTERN-BASED CROSSOVER DETECTOR FOR ROBUST DECODING

One of the advantages of the binary structured-light pattern lies in that it consists of not only intensities but also regularly distributed crossovers. As for the decoding, crossover positions outperform intensities as the former is more resilient to the reflective highlights than the latter. Hence, the crossover positions are more robust and localizable, especially in the presence of reflective highlights.

A. Inverse-Chessboard-Like-Pattern Method for Highlights-Suppression

In our decoding schemes, both the positive and negative patterns are used. Before we extract the crossover position, we subtract the negative images from the positive images, as shown in Fig. 4. This operation makes the crossover extraction and decoding robust. We will explain this as follows.

In the inverse-pattern method, we called the high-frequency patterns directly generated in Section II as positive patterns P . Performing a pixel-wise NOT operation on each positive pattern, we can obtain a set of negative patterns \bar{P} , resulting in the positive captured image L and the negative captured image \bar{L} as shown in Fig. 5.

As discussed in Section II-A, with the proposed high-frequency illuminations, we have $\beta \approx 0.5$. According to (2),

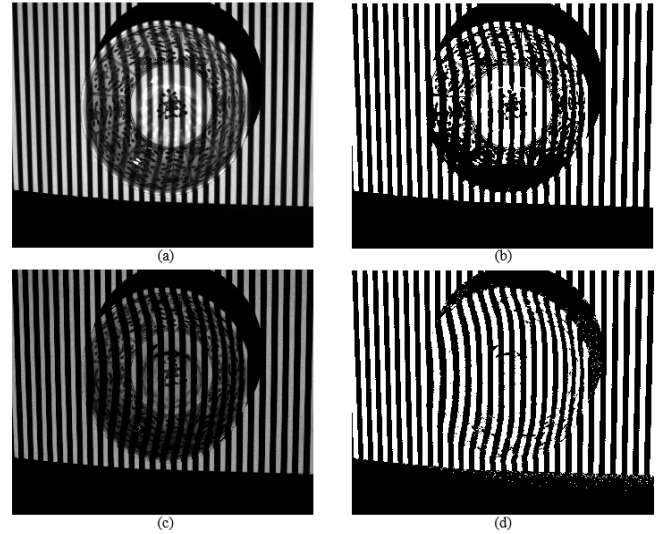


Fig. 6. Inverse-pattern method in the presence of reflective highlights. (a) One of the captured positive images and (b) underlying inaccurate binarization result. (c) One of the highlights-suppression versions of captured images and (d) underlying accurate binarization result.

with $\beta \approx 0.5$, subtracting the negative irradiance \bar{L}^i from the positive irradiance L^i we have

$$D^i = L^i - \bar{L}^i = (L_d^i + 0.5L_g^i) - (1 - 0.5)L_g^i = L_d^i. \quad (4)$$

It can be seen from (4) that the subtraction (difference) results remove the indirect component while preserving the direct component. As the indirect component is the dominant cause for the reflective highlights, in other words, when $\beta \approx 0.5$, positive and negative images contain the same highlights [i.e., see Fig. 5(b)], and hence the subtraction makes sense. After this subtraction, the resulting results can be regarded as a highlights-suppressed version of captured images and are suitable for the further robust crossover extraction.

A schematic example is shown in Fig. 5(b): after subtraction, highlights are canceled out, which stabilizes accurate crossover detection results. It should be noted that this subtraction for highlights-suppression only works when the projected patterns are all-high-frequency patterns, such as the proposed chessboard-like patterns. In contrast, when the pattern is low-frequency, indirect components vary between positive and negative images, compromising the crossover detection results [see Fig. 5(a)]. Hence, conventional gray-code patterns cannot be used in the proposed inverse-pattern method, in which high-frequency patterns are an integral requirement.

Fig. 6 explicitly shows the effectiveness of the proposed inverse-pattern method. One of the captured positive images is shown in Fig. 6(a). The positive image contains both direct and indirect (global) illumination components hence, it has obvious reflections, which leads to inaccurate binarization result as shown in Fig. 6(b). Fig. 6(c) shows the highlights-suppressed version of Fig. 6(a) by employing the proposed inverse-pattern method. In comparison to Fig. 6(a), reflective highlights (global components) are obviously removed while the direct components are well preserved in the meantime. The underlying binarization result of Fig. 6(c) is shown in Fig. 6(d).

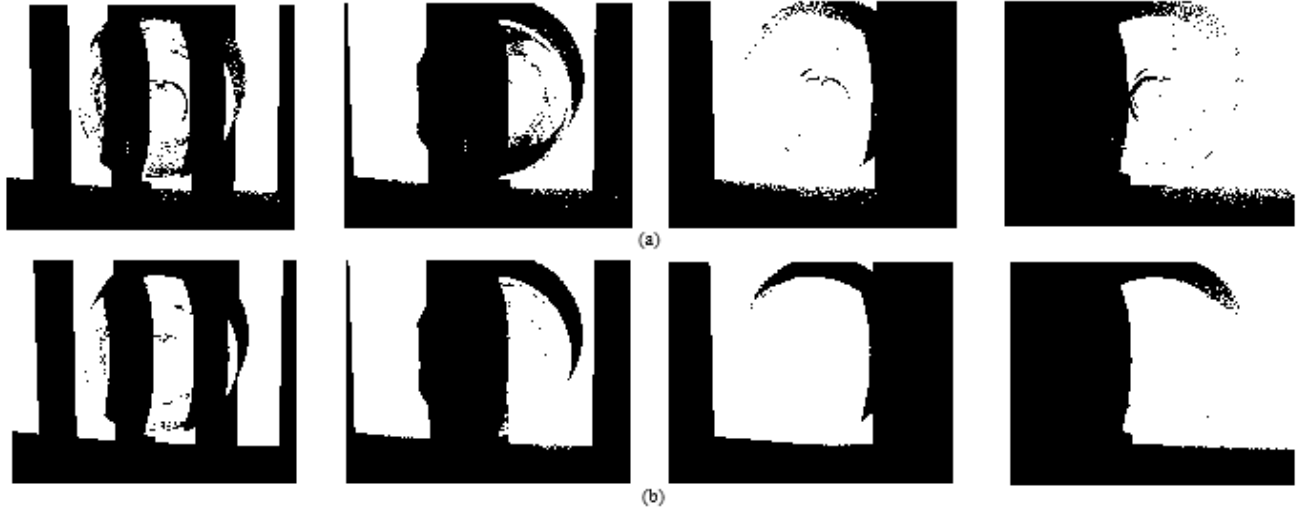


Fig. 7. Partial binarization results by using (a) conventional gray-code method and (b) proposed method. The binarization results of the proposed method are obtained by both combination (XOR) operation and inverse-pattern method. Compared between (a) and (b), reflective highlights lead to fewer binarization errors. In comparison with the four binarization results in (b), it can be seen that binarization errors (decoding errors) are more likely to appear in the least significant bit of decoded results [see the first from left in (b)]. In contrast, the most significant bit of code nearly has no decoding errors [see the last from left in (b)]. Hence, after highlights-suppression of the proposed method, only a few decoding errors remain, which can be easily corrected by an interpolation.

With less disturbance of reflective highlights, a more accurate binarization result can be obtained in Fig. 6(d), compared with the binarization result in Fig. 6(b). More binarization results are shown in Fig. 7.

B. Crossover Detection

An edge detector is used for extracting the edge position in the fringe images. Conventional methods extract the edge position by using a zero crossing of the image intensities, such as the high-order linear filter. Different from the edge detector, as the proposed well-designed chessboard-like coding patterns provide plentiful localizable crossover, we employ the crossover localization method to alleviate the disturbance of surface reflection noise and hence achieve better decoding performance under severe reflection conditions.

Without considering the surface reflection, the crossover can be extracted by the intersection positions of L and \bar{L} . With the disturbance of reflection, an improved crossover detector is proposed, as shown in Fig. 5(b). First, we subtract the negative image \bar{L} from the positive image L ; and obtain the difference pattern $D = L - \bar{L}$. Second, we divide D into positive component $D^+ > 0$ and negative component $D^- > 0$. Finally, the optimized crossover positions along the x axis can be computed by (5). The crossover positions along the y axis can be obtained by replacing the x with y in the following equation:

$$x_{\text{edge}} = (x_{\{\nabla^2 D^+ = 0\}} + x_{\{\nabla^2 D^- = 0\}})/2. \quad (5)$$

It should be noted that the positive pattern P and the negative pattern N have the same high frequency. This same high frequency ensures that the two patterns produce fringe images over which global illumination remains the same for each point in the scene [10]. This enables that the global illumination can be further minimized by the subtraction in D .

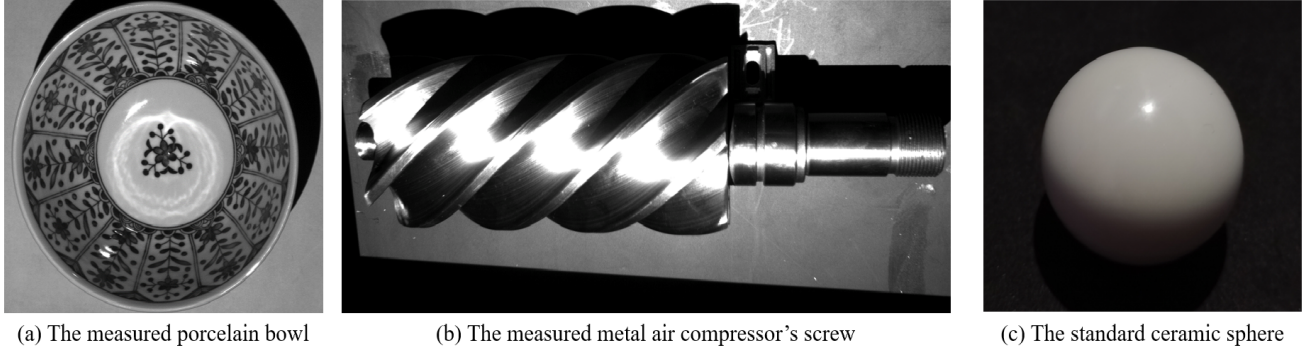
IV. EXPERIMENTAL RESULTS

To evaluate the performance of the proposed method, we performed experiments using three highly reflective objects, including a porcelain bowl, a metal screw, and a standard ceramic sphere (see Fig. 8). These three measured objects are typical and challenging as their surfaces have significant interreflections (highlights). These highlights are undesired in measurement, as they lead to inaccurate binarization results. Also, as the three measured objects (see Fig. 8) have different shapes, the following experiments will illustrate the possible bias of different methods with respect to the actual shape. To illustrate the effectiveness and superiority of the proposed method, we compared the proposed method with Song's inverse-illumination method [4] and Budianto's inpainting method [7]. All algorithms are implemented using a system that consists of a computer with a 4.1GHz CPU and 16GB RAM. The computer is connected to a projector (Texas Instrument DLP4500 with 1280×800 pixels) and a CMOS camera (Flea FL3-U3-13E4C camera with 1280×1024 pixels). The performance of different methods was numerically evaluated by the number of valid measurement points and the measurement accuracy.

A. Qualitative Results

As shown in Fig. 8, even with a small aperture of the lens, there were still reflective highlights (intensity-saturated regions) in the captured image.

In Fig. 9, for the porcelain bowl, the proposed method is compared with the Budianto's inpainting method [7] and the Song's inverse-illumination method [4]. The captured images illuminated by different coding schemas were shown in the first column of Fig. 9. The reflective highlights of the proposed method lighter than that of the two comparative methods, because the proposed chessboard-like patterns are more



(a) The measured porcelain bowl

(b) The measured metal air compressor's screw

(c) The standard ceramic sphere

Fig. 8. Measured objects include (a) porcelain bowl, (b) metal air compressor's screw and (c) standard ceramic sphere. All the three measured objects have challenged high reflections. In comparison to the porcelain bowl, the metal screw has asymmetric geometric structure, resulting in a stronger and more complicated inter-reflection characteristic, and therefore leads to increased difficulty in the structured-lightbased measurement. As the ground-truth of (a) and (b) is difficult to obtain, we use the diameter of the standard ceramic sphere to gauge the measurement accuracy of different methods. In terms of the standard ceramic sphere, the measured scene contains both low reflectance areas (the background) and high reflective area (top of the sphere), both of which are challenging problems that interfere with structured-light measurement.

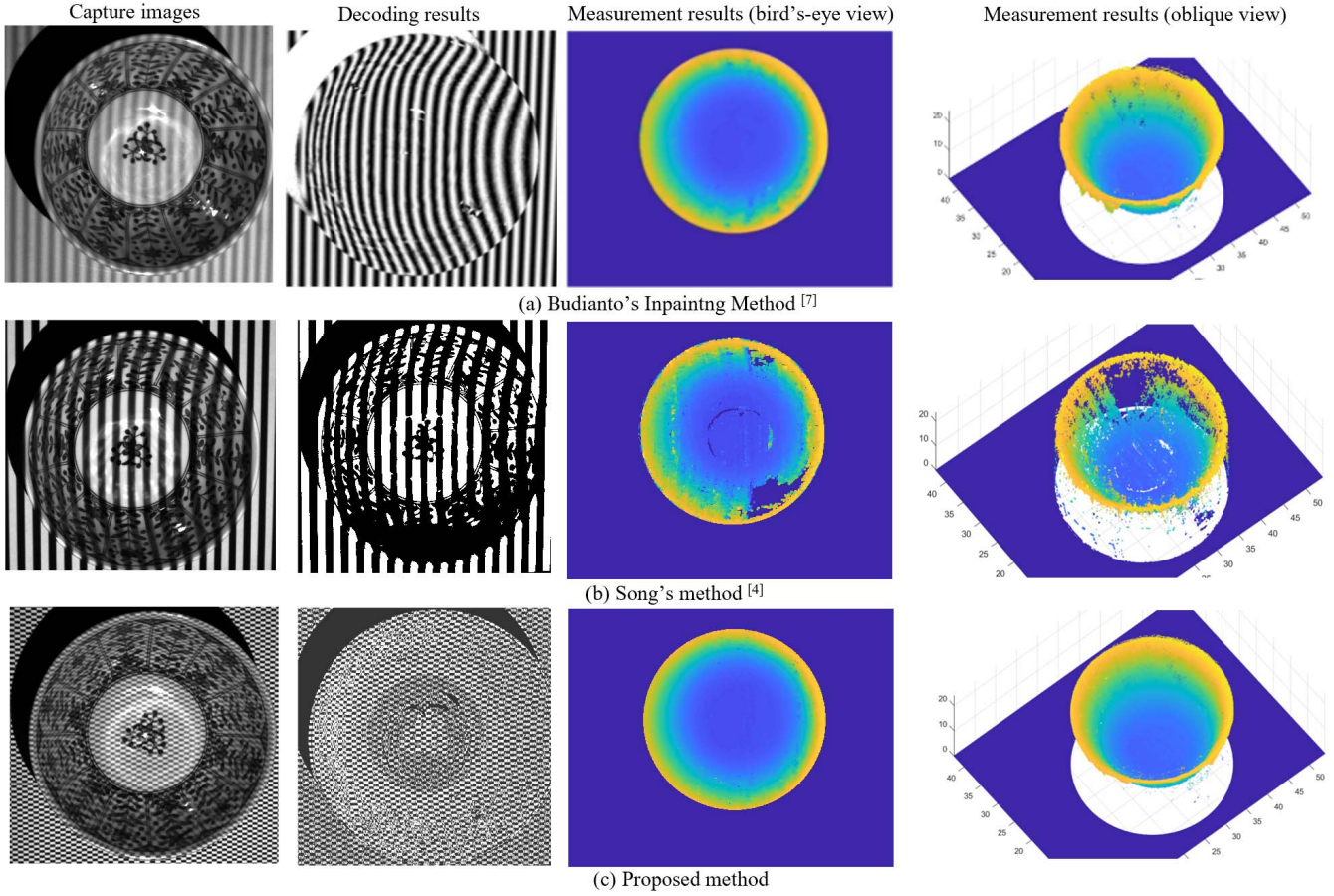


Fig. 9. Measurement result of the porcelain bowl (a) under the Budianto's inpainting method [7], (b) under the Song's inverse-illumination method [4] and (c) under the proposed chessboard-like method. The first column shows one of the captured images of the measured porcelain bowl under different illuminations. The second column shows samples of the decoding results, concretely, the result in (a) is obtained by the geometrically guided-inpainting-based decoding method, the result in (b) is obtained by inverse-stripe-pattern-based decoding method, and the result in (c) is obtained by the proposed inverse-chessboard-like-pattern-based decoding method. The third and the fourth columns respectively show bird's-eye view and oblique view of the measurement results under different methods.

high-frequency and provide better highlights-suppression performance. In Fig. 9, for the symmetrical bowl, the Budianto's inpainting method and the proposed method has better decoding and measurement result than Song's inverse-illumination

method. The Song method is extremely sensitive to surface textures. Dark textures cause large-scale deletions in decoding results and measurement results. In addition to the texture area, the under-exposure area (the area on the lower right

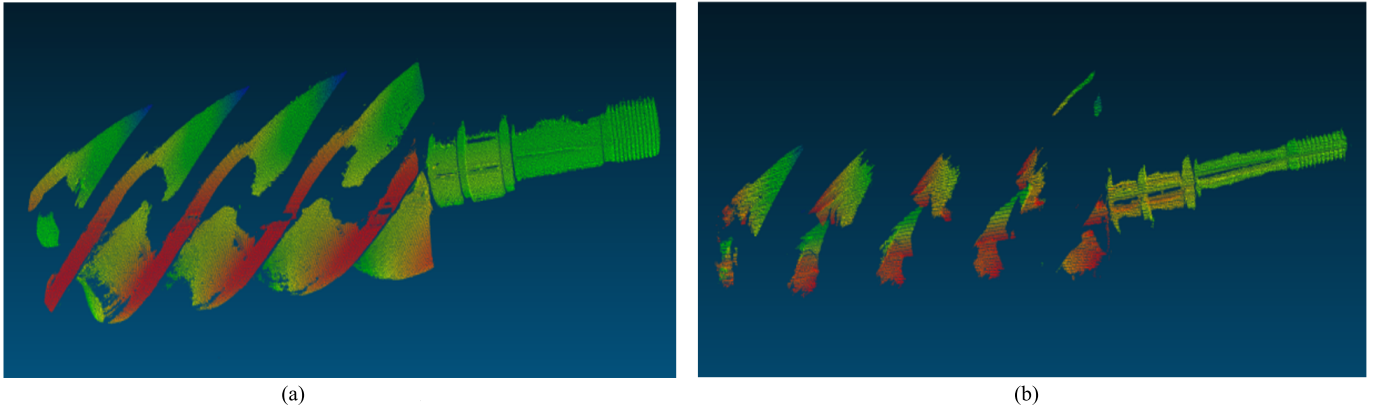


Fig. 10. Measurement results of the metal screw (a) under the proposed method and (b) under the Song's method [4].

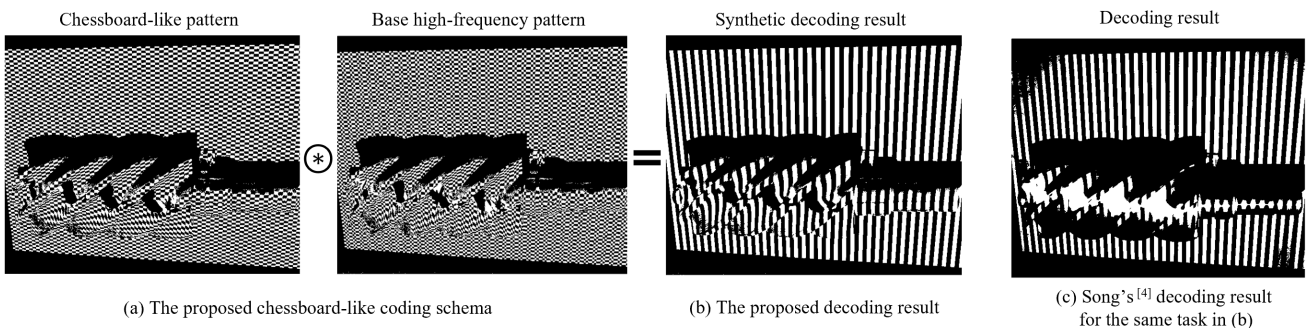


Fig. 11. Comparison of decoding results of (b) proposed chessboard-like coding schema and (c) conventional gray-code coding schema used in song's method [4]. The decoding results show in (b) and (c) correspond to the same encoding template. The experimental details of the proposed chessboard-like coding schema show in (a).

side of the inner wall of the ceramic surface) caused by the combination of highlights and the dynamic range of the camera also has a decoding missing error, resulting in a point cloud hole in the measurement result. For the Budianto's inpainting method, as sinusoidal structured light is not sensitive to the ceramic surface texture, the measurement results is better than Song's method, that is, no texture interference is seen in the phase decoding result, and most of the decoding errors caused by surface reflection are effectively eliminated. However, in areas where there is serious reflection interference at the bottom of the ceramic curved surface and the inner wall, the compensation of the Budianto method fails, resulting in outliers of the measurement point cloud in the failure area, resulting in measurement errors. Compared with Song's and Budianto's methods, the proposed algorithm is robust to texture and reflective interference, and has the best measuring results. In addition, since the proposed algorithm uses a time-domain threshold segmentation method (as described in Section IV-D2), the algorithm in this article can also obtain better measurement results for underexposed areas caused by highlights and camera dynamic range limitations.

In Fig. 10, for the metal screw, we also compared the proposed method with Song's inverse-illumination method [4]. Different from the above-mentioned ceramic curved surface with symmetrical structure, the metal screw not only has high reflective surface materials, but also enhances inter reflections.

The special concave and asymmetric curved surface structure make reflection characteristics extremely complicated. Existing methods generally cannot achieve the measurement of such ultrahigh reflective surfaces, and generally need to be achieved by powder spraying. With Song's method, it can be seen from Fig. 10 that the significant highlights result in obvious measurement errors, only a small part of the screw surface area can obtain effective point cloud information. In contrast, the proposed chessboard-like patterns effectively suppress the adverse effect of highlights on the measurement results, by comparing Fig. 10(a) and (b). Fig. 11 gives the details of the reason that the proposed method outperforms Song's method. As shown in Fig. 11(a) and (b) the proposed method projects two high-frequency chessboard-like patterns to synthesize the decoding results. Compared with Fig. 11(b) and (c), Song's method produces obvious decoding errors at the highlights in the middle of the screw shaft and at the low reflective areas on the outside of the screw, while the proposed chessboard-like-pattern-based method overcomes the disturbance of high reflections and yields a better decoding result.

B. Quantitative Results

In this section, we use both the number of valid points and the measurement accuracy to quantitatively gauge the measurement results of different methods. As the ground-truth

TABLE I
NUMBER OF VALID MEASUREMENT POINTS

Measured Object	Budianto's Method [7]	Song's Method [4]	Proposed
Porcelain Bowl	390572	195599	392589
Metal Screw	-	55104	547161
Standard ceramic sphere	31848	29985	31863

of the porcelain bowl and the metal air compressor's screw (as shown in Fig. 8) is difficult to obtain, we numerically evaluate their measurement results by the valid points, which is used to measure the completeness of the measurement, because the reflection generally causes gross errors such as outliers and missing holes. To further straightforwardly gauge the measurement accuracy, a high-precision standard ceramic ball (sphere) is used (see Fig. 8), as a recognized and widely used standard part for gauging the accuracy.

1) *Number of Valid Measurement Points*: As pointed out in [7], the interference of high reflections on structured-light 3D measurement generally causes gross errors such as outliers, missing holes, etc. Therefore, the number of valid measurement points is an important index to measure and evaluate the performance of different measurement algorithms under reflection interference. We first numerically evaluate the performance of the proposed method by the valid measurement points.

The measurement integrity is defined and measured by the number of valid points in the point cloud measured by the same camera from the same angle of view on the same object. The calculation of the valid points in the measurement point cloud is as follows. Suppose the measurement point cloud is $P = \{p_1, p_2, \dots, p_n\}$, the surface point cloud extracted from the accurate CAD model of the measured object is $Q = \{q_1, q_2, \dots, q_n\}$. Using the closest point iteration algorithm iterative closest point (ICP) to calculate the pose transformation matrix from P to Q , including translation matrix \mathbf{T} and rotation matrix \mathbf{R} , where $q_i = \mathbf{R}p_i + \mathbf{T}$, then the point p_i that meets the following conditions is a valid point

$$\|q_i - (\mathbf{R}p_i + \mathbf{T})\| \leq d \quad (6)$$

where d is the allowable threshold of point cloud deviation, which is 2 mm in our experiment. Count the number of all points satisfying (6) in the measurement point cloud P , and obtain the valid point index which is used to describe the measurement completeness. The above-mentioned ICP algorithm is a widely used point cloud registration algorithm, we implemented it with the help of the algorithm provided in the point cloud processing basic library PCL [22]. For reflective ceramic texture surface (Fig. 9) and metal compressor screw parts (Fig. 10), the number of valid measurement points of different algorithms is shown in Table I.

It can be seen from Table I that for the ceramic texture surface with symmetrical structure and continuous surface, the measurement completeness obtained by the proposed method is slightly better than Budianto's method (completeness improvement 0.52%), and significantly better than Song's

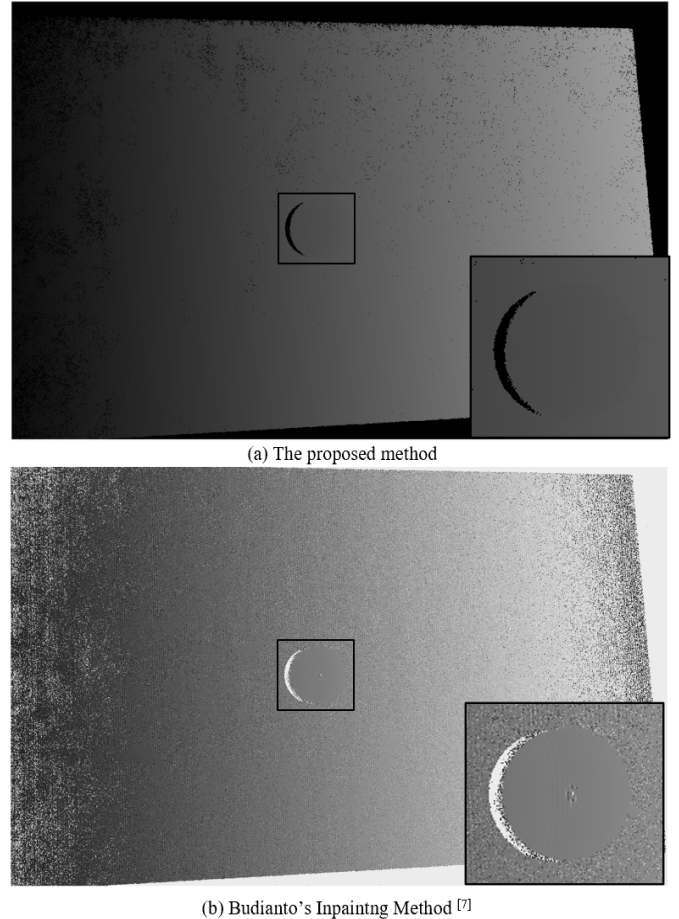


Fig. 12. Comparison of decoding results of (a) proposed chessboard-like method and (b) Budianto's inpainting method [7]. Combined with Fig. 8(c), the proposed chessboard-like-pattern-based method not only has a better decoding result on the highly reflective area of the measured ceramic sphere, but also has a better result on the low-reflective background.

method (integrity improvement 100.71%). In terms of the screw parts of the metal air compressor with complex curvature, as the Budianto method is only suitable for symmetrical continuous surfaces, it fails for the asymmetric metal screw. The Song's method for binary structuredlight projection has a significant lack of point clouds, but the proposed method can still obtain good measurement results. To obtain a more complete measurement point cloud, the proposed method improves the measurement completeness by 892.96% compared with the Song's method. The above numeric analysis results show that the proposed method can obtain good measurement results for highly reflective objects, even textures and underexposed areas with low reflectivity, effectively suppressing the interference of reflections on 3-D measurement, and the proposed method is not subject to the surface shape and structure of the measured object, which has a wide applicability.

Noted that for the standard ceramic sphere, although the number of valid measurement points of the Budianto's method and the proposed method (as shown in Table I) are close, the measurement accuracy of the proposed method is much higher than the Budianto's method, as shown in Table II and discussed as follows. This is because the inaccurate basis of the inpainting methods easily leads to introduce additional

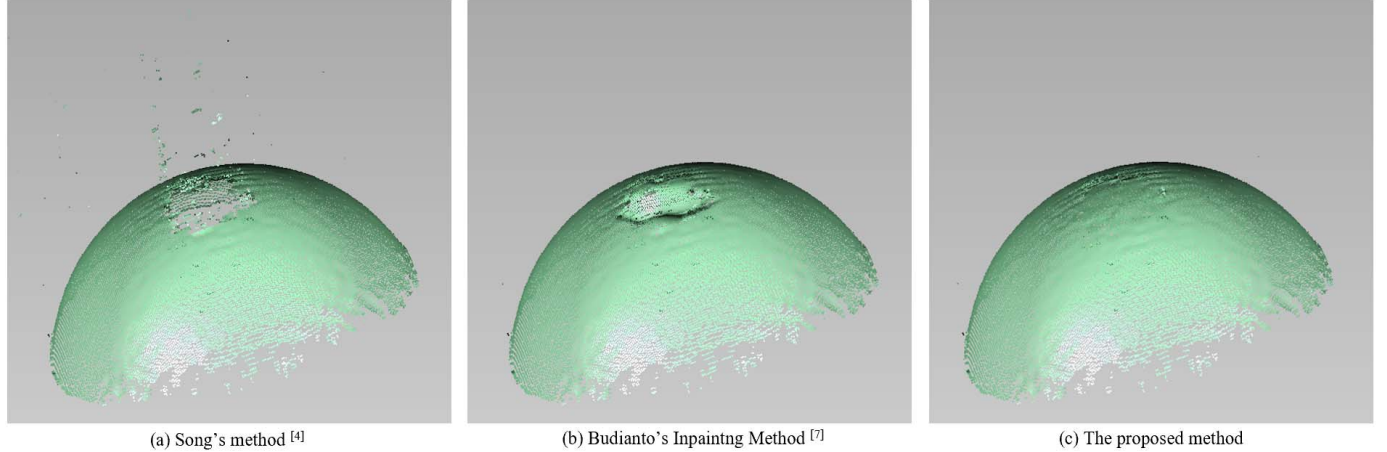


Fig. 13. Measurement result of the standard ceramic sphere under (a) Song's method [4], (b) Budianto's inpainting method [7], and (c) proposed method.

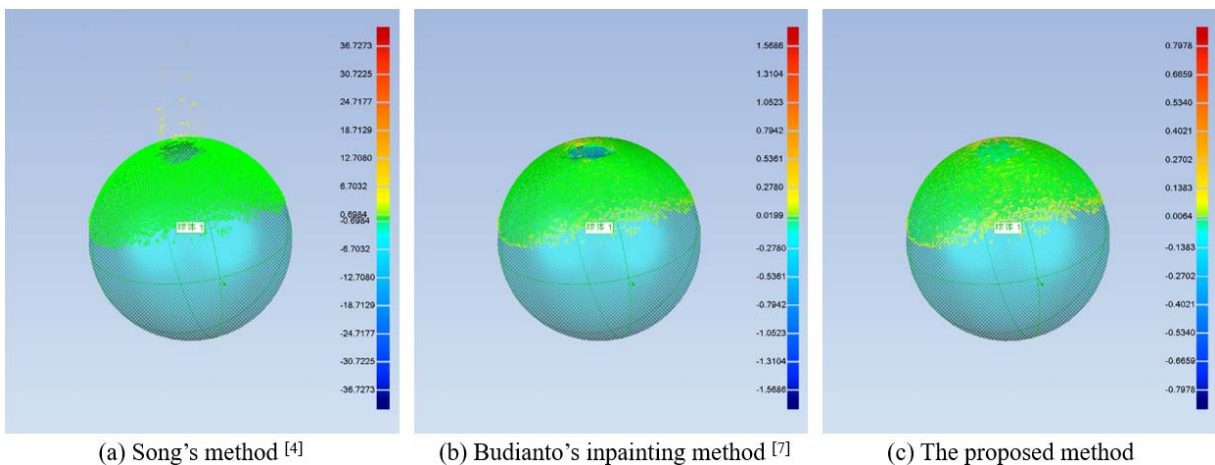


Fig. 14. Measurement deviation of (a) Song's method [4], (b) Budianto's inpainting method [7], and (c) proposed method.

TABLE II
COMPARISON OF MEASUREMENT ACCURACY

Method	Accuracy Index (mm)		
	Fitting Diameter	Maximum Deviation	Standard Deviation
Song's Method [4]	25.0914	27.2356	0.7137
Budianto's Method [7]	25.1221	1.5683	0.1458
Proposed	25.0256	0.3079	0.0357

errors. In other words, Budianto's method has a significant bias with respect to the actual shape, while the proposed method is not affected by the measured surface shape. The shape-independence characteristics of the proposed method will be further analyzed by the measurement accuracy as follows.

2) *Accuracy Analysis:* The measurement accuracy is numerically evaluated with a standard ceramic sphere, as shown in Fig. 8(c). The decoding results of the proposed chessboard-like method and the Budianto's inpainting method are compared in Fig. 12. The proposed chessboard-like-pattern-based method not only has a better decoding result

on the highly reflective area of the measured ceramic sphere, but also has a better result on the low-reflective background. As shown in Fig. 8(c), the measured scene contains both low reflectance areas (the background) and high reflective area (top of the sphere), both of which are challenging problems that interfere with the accuracy of the structured-light 3D measurement. The nominal diameter of the ceramic standard sphere is 25 mm, and the manufacturing accuracy complies the G5 level as the national standard GB/T 308.2-2010, which regulates the change in the diameter of the sphere is not more than 0.25 μm . We also compared the proposed method with the Budianto's inpainting method [7] and the Song's inverse-illumination method [4].

The measurement results and the measurement deviation of different methods were shown in Fig. 13. As shown in Fig. 14, Song's method has the worst measurement results, although it can achieve good measurement results in the lightly reflective area outside the sphere, but it has significant measurement errors (missing and outlier points) in the highly reflective area in the top of the ceramic sphere. The Budianto's method compensates for the missing area of the encoded information in the captured image caused by highlight through image inpainting. Compared with Song's method, although the missing area is

effectively compensated, the compensation result causes local depression, that is, the compensation result is imprecise and introduces additional errors. Applying the proposed method, the reflective interference is significantly eliminated, and there are no voids and isolated points outside the body in the measurement point cloud, and the measurement results are the best. In order to numerically evaluate the measurement accuracy of the measurement results, the diameter of the standard sphere is fitted using the measurement results. And we calculate the deviation between the measurement results and its benchmark the CAD model of the measured object with a diameter of 25 mm, as shown in Fig. 14. The color spectrum on the right side of Fig. 14 intuitively reflects the deviation degree. The diameter fitting results and the measurement deviation (including the maximum and the standard deviation) are shown in Table II. We also give the measurement completeness index in Table II to comprehensively evaluate the measurement performance of different methods.

According to Tables I and II, from the perspective of the measurement completeness, the proposed method eliminates the point cloud voids and external solitary points caused by reflection, and the measurement completeness is the highest. The Budianto's method is equivalent to the proposed method in terms of effective points, but it is easy to see that the compensation result of the Budianto method deviates greatly from the actual surface, and additional errors are introduced. As mentioned above, considering the nominal diameter (25 mm) and manufacturing accuracy of the measured sphere (the variation of the diameter of the sphere is not greater than 0.25 μm), from the perspective of measurement accuracy, the fitting diameter of the algorithm in this article (25.0256 mm) is closest to the diameter of the benchmark, which is better than the fitting diameter of 25.0914 mm by the Song's method, and significantly better than the fitting diameter of 25.1221 mm by the Budianto's method. In addition, the fitting deviation and standard deviation of the proposed method are also the smallest, which shows that the proposed method has the highest measurement accuracy. In summary, compared with the existing methods, the proposed method improves the measurement integrity by reducing the maximum measurement deviation by an average of 89.62% and the diameter fitting accuracy by an average of 75.51%. The proposed method expands the application range and robustness of the structured-light 3D measurement technology.

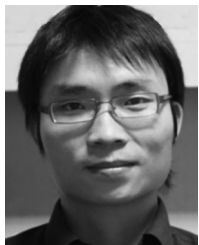
V. CONCLUSION

In this article, a novel method for structured-light measurement in the presence of reflective highlights is proposed. We prevent reflective highlights in both coding and decoding procedures. In the coding procedures, we design high-frequency chessboard-like fringe patterns for the first time to conveniently prevent highlights at capture time itself. A logical combination is used to generate these well-designed patterns. In the decoding procedures, we use the crossover information for decoding, and propose an inverse-pattern method to extract crossover positions. This makes decoding localizable and robust in the disturbance of

reflective highlights. Extensive experiments have been used to demonstrate the high performance of the proposed method in the presence of highlights. Previous methods have also been implemented for result comparison.

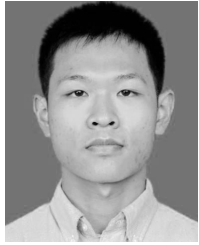
REFERENCES

- [1] P. S. Huang and S. Zhang, "Fast three-step phase-shifting algorithm," *Appl. Opt.*, vol. 45, no. 21, pp. 5086–5091, Jul. 2006.
- [2] Y. Wang, K. Liu, Q. Hao, D. L. Lau, and L. G. Hassebrook, "Period coded phase shifting strategy for real-time 3-D structured light illumination," *IEEE Trans. Image Process.*, vol. 20, no. 11, pp. 3001–3013, Nov. 2011.
- [3] Y. Wang, K. Liu, Q. Hao, X. Wang, D. L. Lau, and L. G. Hassebrook, "Robust active stereo vision using Kullback-Leibler divergence," *IEEE Trans. Pattern Anal. Mach. Intell.*, vol. 34, no. 3, pp. 548–563, Mar. 2012.
- [4] Z. Song, R. Chung, and X.-T. Zhang, "An accurate and robust strip-edge-based structured light means for shiny surface micromeasurement in 3-D," *IEEE Trans. Ind. Electron.*, vol. 60, no. 3, pp. 1023–1032, Mar. 2013.
- [5] J. Salvi, S. Fernandez, T. Pribanic, and X. Llado, "A state of the art in structured light patterns for surface profilometry," *Pattern Recognit.*, vol. 43, no. 8, pp. 2666–2680, Aug. 2010.
- [6] P. Tan, Lin, L. Quan, and H.-Y. Shum, "Highlight removal by illumination-constrained inpainting," in *Proc. 9th IEEE Int. Conf. Comput. Vis.*, vol. 1, Oct. 2003, pp. 164–169.
- [7] D. P. K. Lun, "Inpainting for fringe projection profilometry based on geometrically guided iterative regularization," *IEEE Trans. Image Process.*, vol. 24, no. 12, pp. 5531–5542, Dec. 2015.
- [8] J. Park and A. C. Kak, "3D modeling of optically challenging objects," *IEEE Trans. Vis. Comput. Graphics*, vol. 14, no. 2, pp. 246–262, Mar. 2008.
- [9] S. K. Nayar, G. Krishnan, M. D. Grossberg, and R. Raskar, "Fast separation of direct and global components of a scene using high frequency illumination," *ACM Trans. Graph.*, vol. 25, no. 3, pp. 935–944, Jul. 2006.
- [10] M. Gupta and S. K. Nayar, "Micro phase shifting," in *Proc. IEEE Conf. Comput. Vis. Pattern Recognit.*, Jun. 2012, pp. 813–820.
- [11] M. Gupta, A. Agrawal, A. Veeraraghavan, and S. G. Narasimhan, "A practical approach to 3D scanning in the presence of interreflections, subsurface scattering and defocus," *Int. J. Comput. Vis.*, vol. 102, nos. 1–3, pp. 33–55, Mar. 2013.
- [12] Y. Tang, X. Su, Y. Liu, and H. Jing, "3D shape measurement of the aspheric mirror by advanced phase measuring deflectometry," *Opt. Exp.*, vol. 16, no. 19, pp. 15090–15096, Oct. 2008.
- [13] Y. Xu, F. Gao, and X. Jiang, "Enhancement of measurement accuracy of optical stereo deflectometry based on imaging model analysis," *Opt. Lasers Eng.*, vol. 111, pp. 1–7, Dec. 2018.
- [14] C. Hermans, Y. Francken, T. Cuypers, and P. Bekaert, "Depth from sliding projections," in *Proc. IEEE Conf. Comput. Vis. Pattern Recognit.*, Jun. 2009, pp. 1865–1872.
- [15] T.-C. Hsung, D. P.-K. Lun, and W. W. L. Ng, "Efficient fringe image enhancement based on dual-tree complex wavelet transform," *Appl. Opt.*, vol. 50, no. 21, pp. 3973–3986, 2011.
- [16] W. W.-L. Ng and D. P.-K. Lun, "Effective bias removal for fringe projection profilometry using the dual-tree complex wavelet transform," *Appl. Opt.*, vol. 51, no. 24, pp. 5909–5916, Aug. 2012.
- [17] T. Chen, H.-P. Seidel, and H. P. A. Lensch, "Modulated phase-shifting for 3D scanning," in *Proc. IEEE Conf. Comput. Vis. Pattern Recognit.*, Jun. 2008, pp. 1–8.
- [18] V. Couture, N. Martin, and S. Roy, "Unstructured light scanning to overcome interreflections," in *Proc. Int. Conf. Comput. Vis.*, Nov. 2011, pp. 1895–1902.
- [19] M. Holroyd, J. Lawrence, and T. Zickler, "A coaxial optical scanner for synchronous acquisition of 3D geometry and surface reflectance," *ACM Trans. Graph.*, vol. 29, no. 3, p. 99, 2010.
- [20] A. A. Khorshad, S. N. S. Reihani, and M. T. Tavassoly, "Moiré deflectometry-based position detection for optical tweezers," *Opt. Lett.*, vol. 42, no. 17, pp. 3506–3509, Sep. 2017.
- [21] Z. He, P. Li, X. Zhao, S. Zhang, and J. Tan, "Beyond phase error compensation: Pixel mapping-based error correction for high-accuracy 3D surface measurement," *Meas. Sci. Technol.*, vol. 31, no. 6, 2020, Art. no. 065007, doi: [10.1088/1361-6501/ab6675](https://doi.org/10.1088/1361-6501/ab6675).
- [22] R. B. Rusu and S. Cousins, "3D is here: Point cloud library (PCL)," in *Proc. IEEE Int. Conf. Robot. Autom.*, May 2011, Art. no. 12315963.



Zaixing He (Senior Member, IEEE) received the B.Sc. and M.Sc. degrees in mechanical engineering from Zhejiang University, Hangzhou, China in 2006 and 2008, respectively and the Ph.D. degree from the Graduate School of Information Science and Technology, Hokkaido University, Sapporo, Japan, in 2012.

He is currently an Associate Professor with the Department of Mechanical Engineering, Zhejiang University. His research interests include robotic vision, visual intelligence of manufacturing equipments, and optical-based measurement.



Peilong Li received the B.S. degree in mechanical engineering from Huazhong Agricultural University, Wuhan, China, in 2018. He is currently pursuing the M.S. degree in mechanical engineering with Zhejiang University, Hangzhou, China.

His research interests include structured light-based sensing and machine vision.



Xinyue Zhao received the M.S. degree in mechanical engineering from Zhejiang University, Hangzhou, China, in 2008, and the Ph.D. degree from the Graduate School of Information Science and Technology, Hokkaido University, Sapporo, Japan, in 2012.

She is currently an Associate Professor with the Department of Mechanical Engineering, Zhejiang University. Her research interests include machine vision and image processing.



Lianpeng Kang received the B.S. degree in mechanical engineering from Zhejiang University, Hangzhou, China, in 2019, where he is currently pursuing the M.S. degree in mechanical engineering.

His research interest includes optical-based measurement.



Shuyou Zhang received the M.S. degree in mechanical engineering and the Ph.D. degree from the State Key Laboratory of CAD&CG, Zhejiang University, Hangzhou, China, in 1991 and 1999, respectively.

He is currently a Professor with the Department of Mechanical Engineering, Zhejiang University, where he is also the Administer with the Institute of Design Engineering. His research interests include product digital design, design and stimulation for complex equipments, and engineering and computer graphics.

Dr. Zhang is an Assistant Director of the Computer Graphics Professional Committee for China Engineering Graphic Society, a member of Product Digital Design Professional Committee, and a Chairman of the Zhejiang Engineering Graphic Society.



Jianrong Tan received the B.S. and M.S. degrees in mechanical engineer and electronic engineering from The Open University of China, Beijing, China, in 1982, the M.S. degree in engineering from the Huazhong University of Science and Technology, Wuhan, China, in 1985, and the Ph.D. degree in mathematics from Zhejiang University, Hangzhou, China, in 1987.

He is currently a specially appointed Professor with Zhejiang University, the Doctorial Supervisor and an Academician of the Chinese Academy of Science, the Dean of mechanical engineering, the Associate Supervisor of the CAD&CG State Key Laboratory, the Head of the Institute of Engineering and Computer Graphics, Zhejiang University, and the Chief Supervisor of Engineering Graphics State Fundamental Courses. His researches focus on mechanical designing and theory, and digitalized designing and manufactory. He has authored eight pieces of monograph or compile, 142 pieces of article which has been searched by SCI/EI, which has been cited for 1600 times in the above research areas. He gathered his 15 years' working experience in manufactory and his theory in science, and proposed the technique in combination of batch and customization, which is used for multitudinous customization, the status in engineering transition, the fuzzy status, the technology simulation of random status modeling and digitalized prototype integration, the combination of figures and geometry in multicomponent correlation in intricate equipment, the analysis of multilevel disposing, and multiparameter matching.

Dr. Tan received the National Prize for four times, which includes second prize in National Technology Progress twice, the first prize in National Excellent Education Achievement, he has also got the first prize in provincial level technology progress for six times. He put his technology into the software and got 12 copyrights of computer software, which achieved a lot in manufacturing enterprises.